Upgrading of biomass-derived 2-hexanol to liquid transportation fuels on Cu–Mg–Al mixed oxides. Effect of Cu content

P.J. Luggren, C.R. Apesteguía, J.I. Di Cosimo *

Catalysis Science and Engineering Research Group (GICIC), INCAPE, UNL-CONICET, CCT CONICET Santa Fe, Colectora Ruta Nac. 168, km 0, Paraje "El Pozo", (3000) Santa Fe, Argentina

HIGHLIGHTS

- Cu–Mg–Al mixed oxides promote 2-hexanol upgrading to liquid fuels.
- C9–C24 oxygenates and hydrocarbons are main products.
- ~70% of the products are C9–C15 compounds for jet fuel applications.
- Product quality depends on the Cu content.
- Reaction mechanism changes with the base/metal site ratio.

GRAPHICAL ABSTRACT
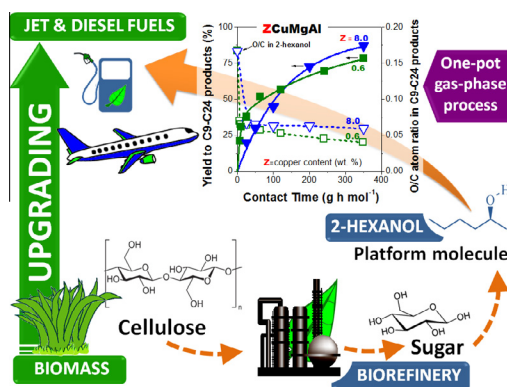
ABSTRACT

The gas-phase synthesis of high molecular weight compounds of application as liquid transportation fuels from 2-hexanol was studied on Cu–Mg–Al mixed oxides with different copper content (0.3–61.2%) and a Mg/Al = 1.5 M ratio. Catalysts were prepared by coprecipitation and characterized by several techniques such as BET surface area, XRD, TPD of CO_2, TPR and N_2O decomposition. Yields of up to 87% were obtained for compounds in the C9–C24 range, ≈80% of which were suitable as jet fuels and the rest as diesel substitutes. This product pool was a hydrophobic mixture of ketones, alcohols and hydrocarbons with 160–200 g/mol average molecular weight and an O/C atomic ratio as low as 0.04. Because low copper content catalysts are hard to reduce, on these materials the reaction occurs via a base-catalyzed mechanism involving consecutive dehydrogenation, C—C bond formation, dehydration and hydrogenation steps, that forms mainly even carbon atom number products. Partially reduced Cu^{n+} atoms contribute to promote a distinct pathway toward odd products. In contrast, on high copper content oxides the reaction yields similar amounts of even and odd products and proceeds by a bifunctional Cu^0-base mechanism in which the C—C coupling is rate-limiting.

© 2016 Elsevier Ltd. All rights reserved.

1. Introduction

In recent years, the increasing energy demand of the emerging economies and the environmental impacts associated with green-house gas emissions resulting from combustion of fossil fuels, among other factors, have motivated the search of new technologies for a sustainable production of transportation fuels. Thus, in the last decades several strategies have been postulated for the use of biomass as a renewable feedstock for this purpose. Unlike fossil fuels, the CO_2 produced during combustion of biomass-derived liquid fuels is consumed during plant growth. However,

the current biofuel production is still far from being considered a carbon neutral technology [1,2]. In addition to the technical advantages, the use of liquid biofuels produced locally would generate geopolitical and social benefits such as the reduction of foreign oil dependency and the strengthening of the job market in the agricultural, forest and fuel sectors [3].

In particular, production of two biomass-derived liquid fuels (biodiesel and bioethanol), the so-called first generation biofuels, has been recently commercially implemented in the transportation sector. However, these solutions face technical limitations related to the blending properties of the resulting biofuel, they represent a small fraction of the total energy contained in the biomass and they require many energy-consuming separation/purification steps. In addition, production of first-generation biofuels entails ethical concerns because of the consumption of edible resources such as sucrose and triglycerides [4,5]. Contrarily, lignocellulose, the most abundant carbohydrate in nature, can be obtained from non-edible sources and therefore, offers an attractive option as an inexpensive feedstock for the efficient liquid fuel production in a biorefinery [6,7].

Lignocellulosic biomass can be treated by different procedures such as gasification, pyrolysis and hydrolysis to obtain by further processing, gasoline, gasoline components and fuels with specific molecular weights, respectively [4,8]. In particular, chemical or biological hydrolysis of lignocellulose is used to separate lignin from sugars. The latter, in turn, can be converted in the biorefinery, resulting in the production of valuable chemicals and transportation fuels [3,9].

Liquid transportation fuels consist of nonoxygenated hydrocarbons in the range of C5–C12 for gasoline, C9–C16 for jet fuel and C12–C20 for diesel [4]. Since sugars have a high O/C atom ratio (O:C = 1:1) which is undesirable for liquid fuel applications, the strategies to convert sugars must include oxygen removal as well as C—C bond formation steps to obtain fuels with appropriate distillation, thermal stability and flashpoint properties as well as the suitable molecular weights for gasoline, diesel or jet fuel applications [4,10].

Several strategies have been postulated for the conversion of carbohydrates such as glucose and xylose into liquid fuels. The primary conversion of these sugars affords formation of hydrogen and functional intermediates by a combination of reforming, reduction and dehydration reactions. These intermediates, so called "platform molecules", comprise C4–C6 oxygenates such as secondary alcohols, ketones, furan-derivatives and acids [4,10,11]. For instance, West et al. [12] studied the transformation of sorbitol and glucose on a PtRe/C catalyst and found that at 100% sugar conversion the resulting organic phase contained ~20% of a mixture of C4–C6 secondary alcohols with 2-hexanol being the main constituent (up to 44% of the total secondary C4–C6 alcohols). Scheme S1 summarizes the biorefinery processing of sugars toward platform molecules, in particular, toward formation of secondary C6 alcohols [10,12]. These platform molecules can be then converted in liquid transportation fuels or fuel additives by different routes such as dehydration, alkylation and aromatization or by C—C bond formation, hydrogenation and hydrodeoxygenation [4,5,11,13]. In particular, Kunkes et al. [10] used bifunctional Cu–Mg–Al mixed oxides, that we had successfully developed years ago for 2-propanol conversion [14], for the upgrading of the C4–C6 fraction to C6–C12 compounds containing one or none oxygen atoms. We showed that Cu–Mg–Al catalysts promote also other reactions such as the gas-phase reduction of α,β-unsaturated ketones by hydrogen transfer reactions [15] and the upgrading of diols to valuable oxygenates [16]. In the last decade, other researchers have shown that similar Cu–Mg–Al mixed oxides are suitable catalysts for C—C coupling of methanol and ethanol [17], aqueous-phase upgrading of bio-oil [18], total oxidation of methane and other VOCs [19–21], synthesis of 1,2-propanediol from glycerol [22], phenol hydroxylation [23] and cinnamaldehyde hydrogenation [24], among many other applications.

Following the approach of Kunkes et al. [10], we recently published our investigations on the synthesis of liquid transportation fuels using 2-hexanol as a model "platform molecule" derived from sugars [25,26]. We reported that the gas-phase conversion of 2-hexanol carried out at 100 kPa and 573 K on Cu-containing mixed oxides with different acid-base properties produces high yields ($\approx$90%) of a mixture of C9–C24 oxygenates and hydrocarbons either under inert or reducing atmosphere (gas-phase H_2). Around 65–75% of the C9–C24 product pool is in the carbon atom range for jet fuel applications. The liquid product has an O/C atomic ratio as low as 0.025. We found that the main reaction pathway toward even carbon atom number products involves tandem dehydrogenation/C—C coupling/dehydration/hydrogenation reactions. However, the reaction pathway shifts toward odd products under operating conditions deprived of gas-phase hydrogen. We elucidated the bifunctional nature of the catalytic process and the participation of Cu^0 and acid-base sites in promoting the different reaction steps. Also, we demonstrated that the relative abundance of these sites determines the rate-limiting step.

In this work we continue our investigations on the 2-hexanol upgrading by oxygen removal and C—C coupling reactions with the aim of stablishing the effect of Cu content on catalyst activity and selectivity. A set of Cu–Mg–Al mixed oxides with a wide range of copper content (0.3–61.2 wt.%) was prepared, characterized by several techniques and tested in the gas-phase conversion of 2-hexanol. The dependence of the reducibility and basic nature of the mixed oxides on the copper loading was studied, as well as how these properties affect the catalytic activity, selectivity and quality of the liquid products. In particular, we investigated how the odd/even carbon atom number product ratio, average molecular weight and oxygen content can be tuned by adjusting the catalyst formulation. The influence of the balance between metal and base sites on determining the rate-limiting step of the bifunctional metal/base mechanism operating at high copper loadings was demonstrated. Furthermore, evidence of the shift to a base-catalyzed mechanism at very low copper contents was provided.

2. Material and methods

2.1. Catalyst synthesis and characterization

Binary or ternary catalyst precursors of Cu-containing mixed oxides were prepared under similar conditions, as detailed elsewhere [14]. In brief, the catalyst precursors consisting of hydroxycarbonates of the metal cations were obtained by co-precipitation; an aqueous solution of the metal nitrates with a total cation concentration of 1.5 M was contacted with an aqueous solution of KOH and K_2CO_3 at a constant pH of 10. All the reagents were analytical grade. After filtering, washing and drying at 363 K, precipitates were decomposed overnight in air at 773 K in order to obtain the corresponding mixed oxide. In particular, a set of 9 ternary Cu–Mg–Al mixed oxides was prepared with a Mg/Al = 1.5 M ratio and different copper contents. These catalysts were denoted as ZCuMgAl, where Z is the copper content expressed in wt.% (Z = 0.3–61.2 wt.%). Another set of mixed oxides was coded as $ZCuM_I(M_{II})$, where M_I and M_{II} stand for metal cations such as Mg^{2+}, Al^{3+}, or Ce^{4+}. Thus, Cu–Mg, Cu–Ce, Cu–Al and Cu–Mg–Ce mixed oxides were obtained.

BET surface areas (*SA*) were measured by N_2 physisorption at its boiling point using an Autosorb Quantachrome 1-C sorptometer. The mixed oxide structural properties were determined by X-ray Diffraction (XRD) technique using a Shimadzu XD-D1 instrument.

The Cu chemical content of the catalyst was analyzed by Atomic Absorption Spectrometry (AAS).

The catalyst base site number (n_b) was measured by temperature-programmed desorption (TPD) of CO_2 preadsorbed at room temperature. Sample was exposed to a flowing mixture of 3% of CO_2 in N_2 until surface saturation. Then, weakly adsorbed CO_2 was removed by flushing with N_2. Finally, the temperature was increased to 773 K at a ramp rate of 10 K/min. The desorbed CO_2 was converted into CH_4 on a Ni/Kieselghur catalyst held at 673 K and then analyzed in a flame ionization detector (FID) [14].

Reduction of the copper phase was studied by temperature programmed reduction (TPR) using 5% H_2/Ar at a flow rate of 50 cm^3/min; the reactor was loaded with an amount of copper (150 µmol) [27] so that to meet the criteria of Monti et al. [28] and Malet et al. [29]. Standard reduction was conducted at a heating rate of 10 K/min from 298 to 653 K. A mass spectrometer (MS) in a Baltzers Omnistar unit monitored the hydrogen consumption. Quantitative H_2-uptakes were calculated by integration of the experimental TPR curves; a previous calibration curve was carried with pure CuO powder (Cicarelli, PA).

The dispersion of the metallic copper particles (D) was measured by a combination of TPR and N_2O decomposition techniques. Two consecutive experiments of TPR were carried out [30]; from the first TPR experiment, Cu_{TPR}^T values in g Cu/g cat were obtained, representing the total amount of reducible copper species up to 653 K. The degree of reduction reached by the sample at 653 K was defined as $Cu_{TPR}^T/Cu_{AAS}^T \times 100$, where Cu_{AAS}^T in g Cu/g cat is the total copper content in the catalyst formulation measured by AAS ($Cu_{AAS}^T = Z/100$). The amount of surface metallic copper (Cu^S) in g Cu/g cat was determined after sample reduction and surface re-oxidation to Cu_2O using N_2O (2 $Cu^0 + N_2O \rightarrow Cu_2O + N_2$). The N_2O decomposition conditions (reaction temperature and pulse volume) were carefully chosen to avoid bulk copper oxidation [31]. Samples were exposed to pulses of N_2O (5×10^{-3} cm^3) at 363 K until surface saturation. The evolved N_2O and N_2 signals were monitored by MS. Then, after flushing with Ar, a second TPR experiment was performed up to 653 K to reduce surface Cu_2O. From the area (A^S) under the TPR curve, the hydrogen uptake was determined and Cu^S was calculated considering the stoichiometry of the reduction reaction ($Cu_2O + H_2 \rightarrow 2Cu^0 + H_2O$) [32,33]. Dispersion was defined as $D = Cu^S/Cu_{AAS}^T = 200 \times A^S \times F \times MW_{Cu}/Z$, where A^S is the area under the TPR curve in Ampere $\times$ s/g cat, F is the calibration factor in mol Cu/(Ampere $\times$ s), MW_{Cu} is the atomic weight of Cu in g Cu/mol Cu. The number of exposed Cu^0 species was calculated as n_{Cu^0} (µmol/g cat) = $157 \times D \times Z$ and the average copper particle size as L (nm) = $6000/(\rho_{Cu} \ S_{Cu}) = 1.04/D$, assuming spherical particles, a copper density $\rho_{Cu} = 8.96$ g/cm^3 and a Cu surface density of 1.47×10^{19} Cu atoms/m^2 [34]; S_{Cu} (m^2/g Cu) = $D \times 6.02 \times 10^{23}/(1.47 \times 10^{19} \times MW_{Cu}) = 644 \ D$ stands for the metallic copper surface area.

Selected samples were analyzed by transmission electron microscopy (TEM) using a JEOL 100 CX II instrument operated at 100 kV.

2.2. Catalytic testing

Vapor-phase conversion of 2-hexanol (C6OL) was carried out at 573 K and 101.3 kPa in a fixed-bed reactor at contact times (W/F_{C6OL}^0) of 6–400 g cat h mol of C6OL^{-1}. Before the catalytic tests, catalysts were pretreated in a flow of N_2 at 773 K for 1 h. Then, the catalyst was reduced in situ in flowing H_2 (35 cm^3/min) at 573 K for 1 h. C6OL (Aldrich $\geqslant$ 98.0%) was introduced via a syringe pump and vaporized into flowing N_2 or H_2 to give a pressure ($\bar{P}_{C6OL}$) of 4.1 kPa. Reaction products were analyzed by on-line gas

chromatography using an Shimadzu GC-2014 chromatograph equipped with flame ionization detector and a (5% Phenyl)-methylpolysiloxane HP-5 Agilent capillary column. Response factors were calculated using the method described by Scanlon et al. [35] and in some cases they were obtained from Dietz [36]. Data were collected every 0.5 h for 5 h. Products were identified using a Varian Saturn 2000 GC/MS with a NIST library of spectra. Details are given elsewhere [25]. Products are denoted as CnO (oxygenates), CnH (hydrocarbons), CnK (saturated ketones), CnUK (unsaturated ketones), CnDK (diketones) and CnOL (alcohols), where n is the carbon atom number in the molecule (n = 3, 6, 9, 12, 15, 18, 21 and 24). Due to a slight catalyst deactivation process, the catalytic results were calculated by extrapolation of the reactant and product concentration curves to zero time on stream (see Fig. S1). Then, X_{C6O}, S and Y represent conversion, selectivity and yield at $t = 0$, respectively. The equilibrated nature of C6OL − C6K interconversions [37] at the present reaction conditions, allows us to consider these two molecules hereinafter as the reactant pool. Thus, conversion was defined for the reactant pool (C6O = C6OL + C6K) as:

$$X_{C6O} = \left(1 - \frac{F_{C6OL} + F_{C6K}}{F_{C6OL}^0}\right)$$

where F_{C6OL} and F_{C6K} are the molar flow rate of C6OL and C6K, respectively, at the reactor exit; F_{C6OL}^0 is the molar flow rate of C6OL in the reactor feed.

Product selectivity was calculated on a carbon atom basis, as:

$$S_i = \frac{F_i N_i}{\Sigma F_i N_i}$$

where N is the carbon atom number of product "i". Carbon balances closed to within 90–98% (an example is given in Fig. S2).

Site time yield (STY_i) is defined as the moles of product "i" per mole of Cu^0 surface site and per second.

3. Results and discussion

3.1. Characterization of the ZCuMgAl mixed oxides

Catalysts combining a metallic function provided by Cu^0 atoms and acid-base sites supplied by Lewis acid cations were prepared by coprecipitation and characterized by several techniques. They were denoted as $ZCuM_I(M_{II})$, where Z represents the copper content in wt.% and M_I and M_{II} are the accompanying cations (Mg^{2+}, Al^{3+} or Ce^{4+}). Binary Cu–Mg, Cu–Ce and Cu–Al, and ternary Cu–Mg–Ce mixed oxides containing similar copper loadings were denoted as 9.8CuMg, 7.4CuCe, 6.4CuAl and 6.9CuMgCe, respectively. In particular, 9.8CuMg and 6.4CuAl catalysts were prepared to represent typically, bifunctional metal-base or metal–acid catalysts, respectively. A detailed characterization of these materials is given in a previous work [25].

Another set of ZCuMgAl mixed oxides having a Mg/Al = 1.5 (molar ratio) was prepared. Mg^{2+} and Al^{3+} were selected because of the known catalytic performance as basic and acidic catalysts, respectively, of their corresponding single oxides in the conversion of different alcohols and polyols [38–41]. In these materials Z was varied in a wide range between 0.3 and 61.2 wt.% Cu. The physicochemical properties of the ZCuMgAl oxides prepared in this work are summarized in Table 1. Elemental analysis revealed that the measured Cu loadings were in all cases very close to the nominal values, therefore confirming complete precipitation of the cations during the synthesis procedure.

Thermal decomposition of the precipitates at 773 K under air removes water and CO_2 and generates the porous structure that is responsible for the high mixed oxide surface area (SA) [41]. SA

Table 1
Physicochemical properties of ZCuMgAl catalysts.

Catalyst (Z: wt.% Cu)	Surface area, SA (m²/g)	Nominal composition (wt.%)			Structural analysis by XRD		Cu species reducibility, dispersion and size				Basic properties	
		Cu	Mg	Al	a_{MgO}[a] (Å)	Phases detected	D[b] (%)	n_{Cu^o}[c] (µmol/g)	L[d] (nm)	T_M[e] (K)	n_b[f] (µmol/g)	BS[g]
0.3CuMgAl	217	0.5	32.9	23.7	4.167	MgO	–	–	–	–	527	1.07
0.6CuMgAl	260	0.8	32.7	23.6	4.172	MgO	–	–	–	–	532	1.01
1.2CuMgAl	294	1.0	32.7	23.6	4.170	MgO	–	–	–	681	511	0.98
1.8CuMgAl	225	2.0	32.2	23.2	4.167	MgO	–	–	–	658	497	0.60
4.1CuMgAl	230	4.2	31.4	22.6	4.171	MgO	16.9	109	6.1	586	413	0.64
8.0CuMgAl	248	10.0	29.0	20.9	4.150	MgO	12.2	153	8.5	571	457	0.49
15.1CuMgAl	208	15.0	26.9	19.3	4.145	MgO–CuO	10.2	242	10.2	539	412	0.48
32.7CuMgAl	90	35.0	18.6	13.3	4.145	MgO–CuO	5.6	287	18.6	506	225	0.34
61.2CuMgAl	42	70.0	4.1	2.9	–	CuO	4.4	421	23.8	493	66	0.20

[a] MgO lattice constant.
[b] Cu^0 dispersion by N_2O decomposition.
[c] Number of exposed Cu^0 atoms.
[d] Cu^0 particle size.
[e] Temperature at peak maximum by TPR.
[f] Base site number by TPD of CO_2.
[g] Basic strength defined in Section 3.1.

values were independent of the copper content for Z ⩽ 15.1 wt.% but decreased notoriously at higher loadings. The latter is attributed to the low aluminum content of these oxides; Al is a textural promoter in Mg–Al or Cu–Zn–Al catalysts that helps stabilize the porous structure and facilitates dispersion of the copper particles [41,42].

The structural analysis and the identification of the crystalline phases present in the ZCuMgAl oxides were carried out by XRD (diffractograms shown in Fig. S3). A single quasi-amorphous MgO (periclase, ASTM 4-0829) phase was detected at low copper contents (Z < 15.1 wt.%) but at higher Z values a CuO (tenorite, ASTM 5-0661) phase was clearly identified. No crystalline Al-containing phase was detected at any Z value indicating that the Al^{3+} cations remain closely associated with the MgO structure after calcination, in agreement with previous work [41]. In fact, incorporation of the Al^{3+} cations in the MgO matrix is evident in the MgO lattice parameter (a_{MgO}), Table 1. The lower a_{MgO} values in the ZCuMgAl oxides compared with that of pure MgO (4.216 Å) reveal a contraction of the MgO unit cell as a result of substitution of smaller Al^{3+} cations ($r_{Al^{3+}}$ = 0.535 Å) for Mg^{2+} ($r_{Mg^{2+}}$ = 0.72 Å) in the structure.

The fact that no crystalline copper species was detected at low Z values indicates that the Cu cations are forming highly dispersed CuO crystallites not detectable by XRD or they are incorporated as a solid solution within the oxide lattice. To get insight into this issue, the reducibility of Cu species in ZCuMgAl samples was investigated by TPR, Fig. 1. A single and broad reduction peak centered at around 500–600 K was observed for Z ⩾ 4.1 wt.%. The TPR curve of sample 8.0CuMgAl carried out up to 1073 K confirms the lack of species reducing at higher temperatures in this compositional range. In line with that, calculation of the amount of reducible copper species (Cu_{TPR}^T) indicate that for Z = 4.1–61.2 wt.% Cu the degree of reduction was 100%, i.e., reduction of all the Cu atoms in these samples took place below 653 K. Contrarily, for samples with lower copper loadings (Z < 4.1 wt.%), reduction was not complete at 653 K; less than 30% of the total copper atoms were reduced at that temperature. In particular, the TPR pattern of sample 1.2CuMgAl carried out up to 1073 K shows that part of the Cu atoms reduces at ≈850 K.

In Fig. 1, the shift of the temperature at the peak maximum (T_M) to lower values as Z increases suggests a diminution of the Cu-mixed oxide interaction resulting from segregation of CuO species. On the other hand, the presence of hardly-reducible copper species in Cu–Mg–Al solid solutions explains the higher T_M values for low metal loading catalysts (Z < 4.1 wt.%) [42,43].
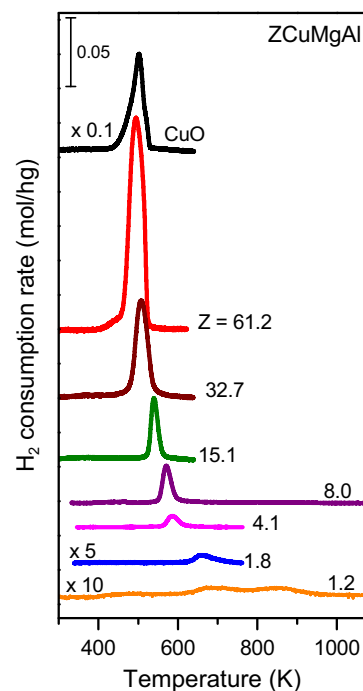

Fig. 1. TPR profiles of ZCuMgAl oxides.

Indeed, participation of Cu in formation of a solid solution can be inferred from the calculations of a_{MgO} in Table 1. Solubility of the Cu^{2+} ions within the MgO structure is favored by the slight difference in ionic size between octahedrally coordinated Cu^{2+} ($r_{Cu^{2+}}$ = 0.73 Å) and Mg^{2+} in MgO ($r_{Mg^{2+}}$ = 0.72 Å) [44]. Thus, substitution of small amounts of Cu^{2+} for Mg^{2+} ions within the periclase structure results in a small expansion of the MgO lattice (higher a_{MgO} values) at low Cu loadings.

Copper dispersion (D) was calculated by combining TPR and N_2O decomposition experiments in a two-step procedure as described in Section 2.1. D values between 4% and 17% were obtained for ZCuMgAl samples with copper loadings Z ⩾ 4.1 wt. %, Table 1; these results were similar to values reported in the literature for comparable Cu-based oxides [45–48]. Below that copper content, meaningful dispersions could not be measured because of experimental limitations to operate under conditions

free of artifacts [28]. The Cu[0] particle size (*L*) and the number of exposed Cu[0] species on the surface (n_{Cu^0}, μmol/g) were calculated from the *D* values, Table 1; n_{Cu^0} (Fig. 2) monotonically increased with increasing the Cu content in a similar fashion to *L*. Thus, at high Z values the oxide surface contains more and larger reduced copper species.

The surface basic properties of the ZCuMgAl samples were investigated by TPD of CO_2, Fig. 3. By integration of the TPD curves, the number of base sites (n_b) was calculated and results are shown in Table 1. In Fig. 3, reference samples such as 9.8CuMg and 6.4CuAl were also included; they represent a strongly basic and a weakly basic material, respectively. The former presents basic features comparable to those of MgO with CO_2 desorbing in a wide temperature range (350–700 K). On the other hand, in sample 6.4CuAl the lack of Mg^{2+} cations makes CO_2 desorb at lower temperatures (~400 K), presenting basic features comparable to those

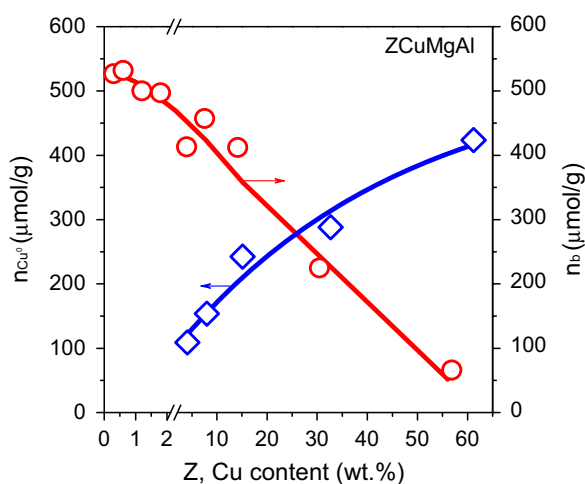**Fig. 2.** Number of base (n_b) and metal (n_{Cu^0}) sites of ZCuMgAl oxides as a function of the copper content (Z).

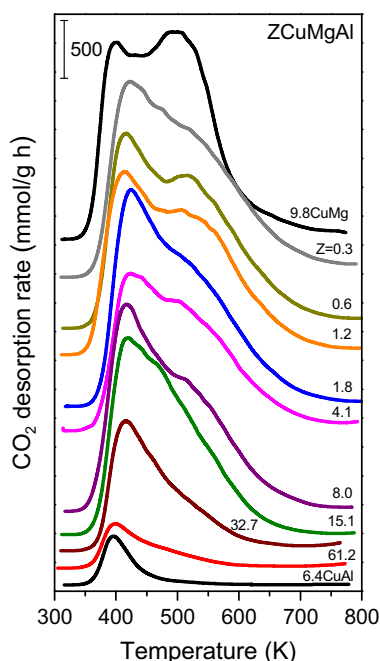**Fig. 3.** TPD of CO_2 of ZCuMgAl, 9.8CuMg and 6.4CuAl oxides.

of Al_2O_3 [16]. Clearly, the basic properties of the ZCuMgAl oxides are between those of the reference materials. The shape of the TPD curves for the ZCuMgAl oxides, that reflects the base strength distribution, was similar for all of them. However, the high-temperature peak at ~550 K gradually disappeared as Z increases indicating a diminution of the overall basicity because of the reduced contribution of strong base sites.

Based on previous work on basic oxides [40,41], the TPD profiles of Fig. 3 were deconvoluted in three desorption bands, reaching maximum desorption rates at about 400, 450, and 550 K. Thus, the contribution of each band identified as the number of weak (n_W), medium (n_M) and strong (n_S) base sites, respectively, was calculated. An indication of the sample basic strength (*BS*) was defined as $BS = n_S/(n_W + n_M)$ and the values are reported in Table 1. On the low Cu content materials, *BS* is enhanced by a factor of 5 compared to samples with high Z. Although the Mg/Al ratio is constant in all the ZCuMgAl samples, the decreasing Mg content as Z increases (with the consequent segregation of more electronegative Cu^{2+} cations on the oxide surface) is detrimental to the solid overall basic strength. Blocking of the surface base sites and formation of more acidic CuO surface patches explain the poor basic properties of the high copper loading samples.

Fig. 2 shows that in the ZCuMgAl catalysts the contribution of surface basic and metallic sites strongly depends on the copper content and that n_b decreases linearly with Z.

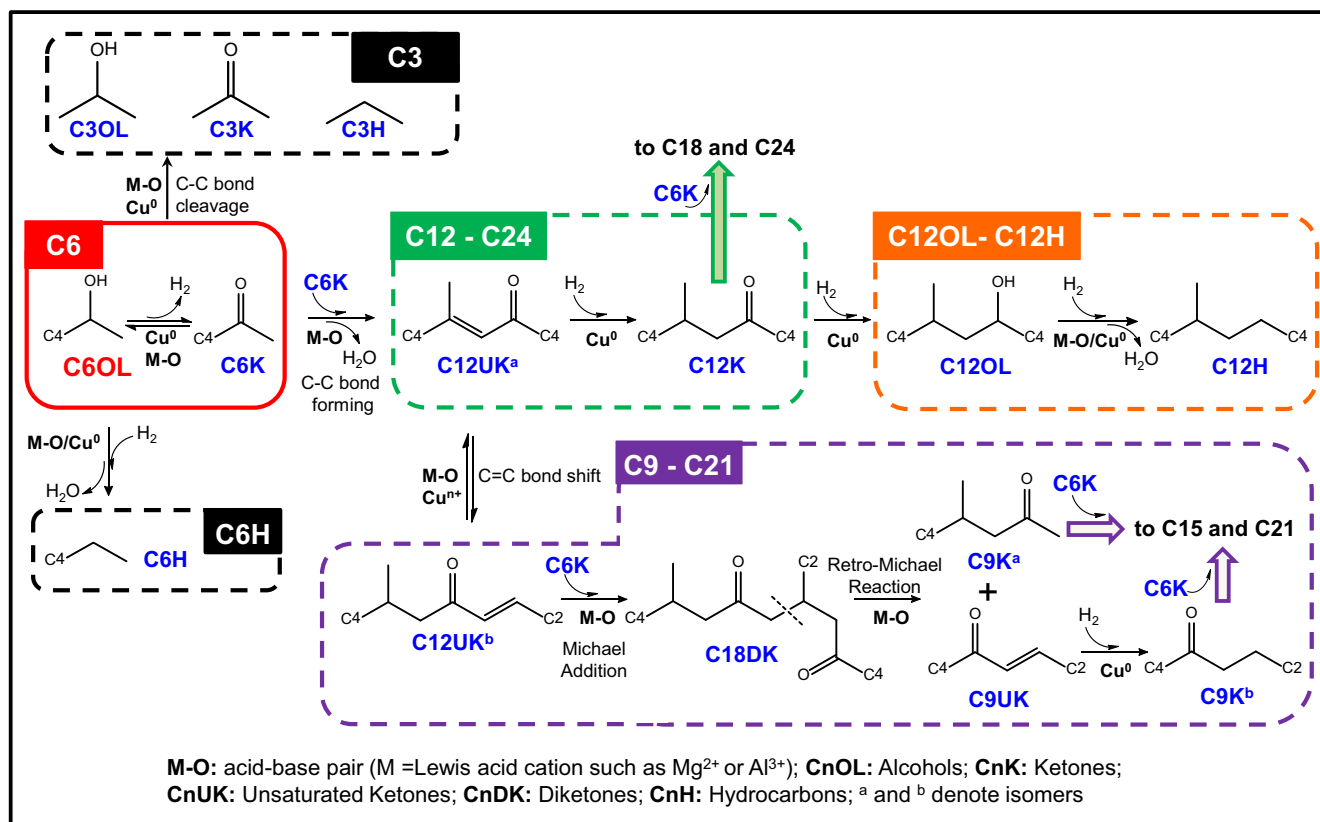### 3.2. Catalytic results. Effect of the copper content of ZCuMgAl catalysts

Liquid transportation jet or diesel fuels are a hydrophobic mixture of C9–C18+ compounds with a low O/C atom ratio. In a previous work [25] we showed that 2-hexanol (C6OL) can be converted in the gas phase into branched hydrocarbons, ketones and alcohols having carbon atom numbers in the range of $n = 3 - 24$ (C3–C24). More than 70% of these products were in the C9–C15 range.

We also studied the reaction pathways leading to C9–C18+ compounds from C6OL; we found that they involve a series of consecutive reaction steps comprising dehydrogenation, C—C coupling, dehydration and hydrogenation reactions, Scheme 1 [26]. The sequence depicted in Scheme 1 starts by C6OL dehydrogenation to C6K (block C6). Surface-generated hydrogen during this step is the only source of reducing agent in the reaction system. Hydrogen is needed to reduce C=C and C=O bonds in the following steps.

In the initial steps C6OL may also dehydrate-hydrogenate to hexane (C6H) (block C6H) or undergo C—C bond cleavage toward formation of short chain compounds such as C3OL, C3K and C3H, (block C3). However, C3 and C6H products are unwanted for liquid fuel applications. Thus, the best selectivities to valuable products (C9–C24) were obtained on catalysts having a high base/acid site ratio (n_b/n_a). In contrast, catalysts with a low n_b/n_a ratio mainly convert C6OL to C6H.

The reaction then proceeds by C–C bond forming aldol condensation of C6K giving rise to an aldol adduct (a hydroxyketone, not shown) that is easily dehydrated to the α,β-unsaturated ketone C12UK[a]. Sequential formation of other C12 products (C12K, C12OL and C12H in Scheme 1) then occurs by a series of hydrogenation and dehydration steps. The carbon chain can be lengthened further by reaction of C12K with another C6K molecule to give ketones, alcohols and hydrocarbons with an even number of carbon atoms, such as C18 and C24.

A reaction sequence was postulated in which formation of odd carbon atom number compounds (block C9–C21) proceeds through a distinct reaction pathway, Scheme 1; it starts by the C=C bond shift in the α,β-unsaturated ketone C12UK[a] giving the isomer C12UK[b]. Formation of C9K occurs then by consecutive Michael [49,50] and retro-Michael reactions, after which conventional aldol

M-O: acid-base pair (M = Lewis acid cation such as Mg^{2+} or Al^{3+}); **CnOL:** Alcohols; **CnK:** Ketones; **CnUK:** Unsaturated Ketones; **CnDK:** Diketones; **CnH:** Hydrocarbons; [a] and [b] denote isomers

Scheme 1. Reaction steps for the conversion of C6OL on ZCuMgAl catalysts.

condensation steps lead to C15 and C21 products. In particular, we found that the pathway to even carbon atom number compounds was favored when the reactant was diluted in hydrogen. In contrast, odd carbon atom number compounds prevailed when only surface-generated hydrogen is available, such as under inert atmosphere.

Using mixed oxide catalysts with ≈8 wt.% Cu and different acid-base properties we found that Cu-containing solids were more selective to produce C9–C24 compounds than the corresponding Cu-free oxides. This was explained by identifying the role played by the different active sites, so that highly dispersed Cu^0 species promote the C6OL dehydrogenation at high rates whereas acid-base sites mainly participate in the aldol condensation steps. Thus, we concluded that bifunctional catalyst formulations combining acid-base sites with moderate basic properties and dispersed Cu^0 sites were suitable for the efficient synthesis of liquid fuels.

Here we continue our investigations on the conversion of C6OL toward C9–C18+. The ZCuMgAl catalysts with $Z = 0.3 - 61.2$ wt.% Cu were tested in the reaction at 573 K in order to elucidate the effect of the copper content on the catalyst activity and product distribution. The reactant pool conversion rate (r_{C6O}, mmol/h g cat) as well as the selectivity to C3 (S_{C3}), C6H (S_{C6H}) and C9–C24 compounds (S_{C9-C24}) at 20% conversion are shown in Fig. 4. Fig. 4A shows that r_{C6O} decreased with increasing Z in a similar fashion as n_b in Fig. 2. Thus, samples with enhanced basic properties are more active.

As shown in Fig. 4B, S_{C9-C24} was more than 80% on all the ZCuMgAl catalysts and slightly increased with Z reaching ≈95% on the high copper content samples. Thus, it seems that the pathway toward heavy compounds, Scheme 1, requires a high number of Cu^0 species, Fig. 2. An opposite trend was found for S_{C6H}; low copper content catalysts, where surface Cu^0 species are less abundant, initially dehydrate C6OL on the acid-base sites giving

C6 hydrocarbons (C6H) in agreement with previous work on alcohol dehydration reactions [51]. All these results are explained by the preference of the surface Cu^0 species to activate the O—H bond over the C—O bond of C6OL in the initial reaction step, therefore favoring the dehydrogenation pathway that starts the aldol condensation sequence. On the other hand, the S_{C3} values were negligible regardless of the Z value what means that the C—C bond breaking of the C6O pool is not a relevant reaction.

The O/C atom ratio is 0.8 in cellulose [52], 1.0 in monosaccharide sugars, and 0.167 in the reactant C6OL. Fig. 4B shows that the calculated O/C atom ratio in the C9–C24 product pool obtained on ZCuMgAl catalysts can be decreased to ≈0.07 at 20% conversion. This low value confirms that upgrading of C6OL through the reaction sequence depicted in Scheme 1 gives a product mixture with superior hydrophobic properties than C6OL. The O/C ratio was similar irrespective of the copper content because the oxygenates/hydrocarbons ratio in the C9–C24 product pool was independent of Z at that low conversion level.

At 20% conversion, the C9–C24 fraction contains mainly C12 compounds and to a lesser extent, C9 and C15 products; Fig. 4C shows the evolution of the selectivity toward odd (C9, C15 and C21) and even (C12, C18 and C24) carbon atom number products as Z increases. At low Z values the ZCuMgAl samples converted C6OL mainly to even products but for Z > 4.1 wt.% Cu comparable selectivities to odd and even products were obtained.

The effect of varying Z was also investigated at higher conversions levels. Contact times (W/F^0_{C6OL}) were gradually increased up to 350 gh/mol in order to reach almost complete conversion (93%). Two samples were selected for these experiments: 0.6CuMgAl, representing the compositional zone of the very active (Fig. 4A), strongly basic (Fig. 3) and hardly reducible oxides, and 8.0CuMgAl, corresponding to oxides with moderate activity (Fig. 4A), basic properties (Table 1) and number of surface metallic
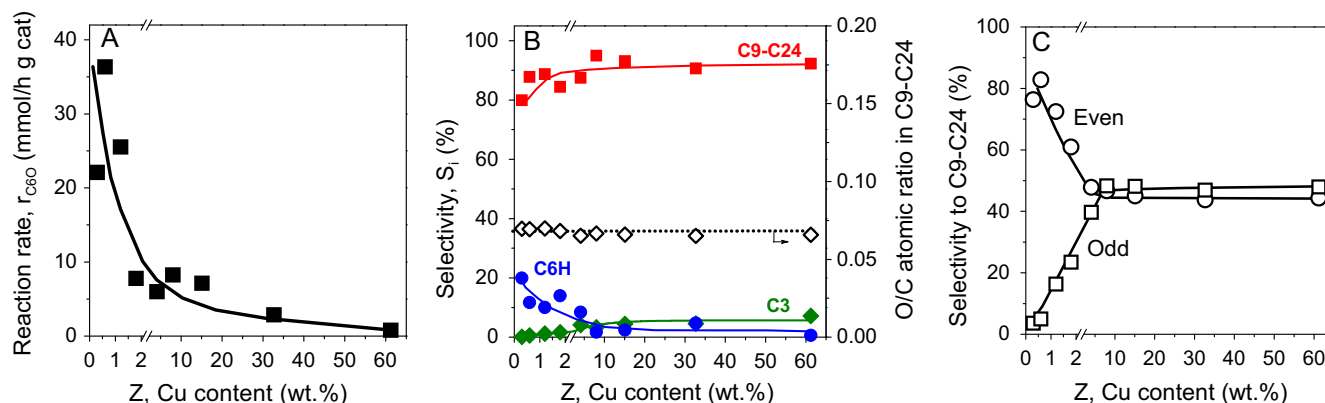
Fig. 4. Catalytic results as a function of copper content (Z). (A) Reaction rate; (B) selectivity to C9–C24, C6H and C3 products and O/C atom ratio in C9–C24 products; (C) selectivity to odd and even carbon atom number products in the C9–C24 pool [T = 573 K, P = 101.3 kPa, $\overline{P}_{C6OL}$ = 4.1 kPa; N_2 balance; X_{C6O} = 20%].

sites (Fig. 2). Fig. 5 shows conversion (X_{C6O}) and yield (Y_i) to different products as a function of W/F^0_{C6OL}. The local slopes of the yield curves represent formation rates. In sample 0.6CuMgAl, Fig. 5A, the change of the slope of the Y_{C9-C24} curve at W/F^0_{C6OL} > 50 gh/mol is probably due to a hydrogen deficiency at high conversions since part of the reactant C6OL is dehydrated to C6H instead of being converted to C6K and hydrogen. Furthermore, because of the low Z value the amount of reducible Cu species that perform C6OL dehydrogenation is low but several hydrogen molecules are needed to form C9–C24 products, Scheme 1. Thus, it seems that surface-generation of hydrogen takes place anyway as indicated by the high Y_{C9-C24}.

We showed previously that basic catalysts dissociate the O—H and C—H bonds of secondary alcohols giving ketones and hydrogen but at a much lower rate than metallic catalysts [14,38,51]. Thus, the base sites of the 0.6CuMgAl sample probably contribute to dehydrogenate C6OL and retain the generated surface hydrogen fragments that migrate and reduce the C=C bond of C12UK[a] giving C12 K; C12 compounds then initiate the pathway toward heavier compounds. To confirm that the lack of enough surface hydrogen fragments causes the reaction to slow down at high conversions, an additional experiment was carried out diluting C6OL in pure H_2 (open symbols in Fig. 5A); clearly, X_{C6O} and Y_{C9-C24} increased indicating that the pathway from C6K to C12 and heavier products is favored when gas-phase hydrogen is supplied to the reactor. Thus, the abundant base sites of sample 0.6CuMgAl likely partici-

pate in H—H bond dissociation and subsequent hydrogenation steps. These results are supported by previous findings; we showed time ago that the strongly basic sites of MgO dissociate $H_2(D_2)$ at high rates during H_2–D_2 equilibration reactions [53]. A similar experiment was carried out with sample 8.0CuMgAl (open symbols in Fig. 5B), however in this case the result is predictable since the high n_{Cu^0} of this sample is expected to facilitate hydrogen dissociation and incorporation of hydrogen fragments in the reduction steps leading to C9–C24 compounds, Scheme 1.

Despite of the differences in the C9–C24 product formation rate at low W/F^0_{C6OL} values, the highest Y_{C9-C24} was almost the same on both samples (80–90%). Furthermore, none of the catalysts formed significant amounts of unwanted C3 products at any conversion level. However, the main difference between the two samples was the amount of products with an odd number of carbon atoms formed from C6OL. Fig. 6 (closed symbols) shows the ratio of Odd/Even carbon atom number products in the C9–C24 pool for the reactions carried out on 0.6CuMgAl and 8.0CuMgAl. The ratio on 8.0CuMgAl was ~1.0, reflecting that the pathways toward odd and even products of Scheme 1 proceed with similar selectivity regardless of the conversion level. In contrast, sample 0.6CuMgAl formed mainly C12 products (S_{C12} = 80%) at low conversions, but these compounds further converted to increasing amounts of odd products at higher conversions. Thus, the Odd/Even ratio gradually increased from 0.06 reaching a value of 0.44 at high conversion levels. The surface of sample 0.6CuMgAl is deprived of hydrogen
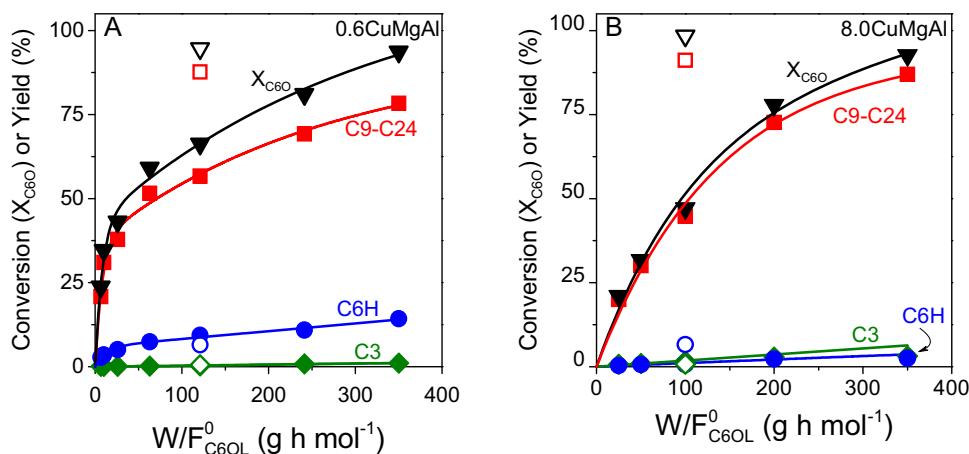
Fig. 5. Conversion and product yield as a function of contact time (W/F^0_{C6OL}) on (A) 0.6CuMgAl; (B) 8.0CuMgAl. Closed symbols: inert atmosphere; open symbols: H_2 atmosphere [T = 573 K, P = 101.3 kPa, $\overline{P}_{C6OL}$ = 4.1 kPa].
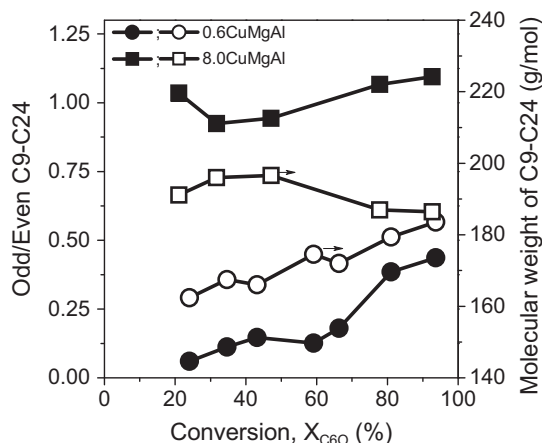
Fig. 6. Ratio of Odd/Even carbon atom number products and average molecular weight of the C9–C24 product pool as a function of conversion for 0.6CuMgAl and 8.0CuMgAl catalysts [T = 573 K, P = 101.3 kPa, $\bar{P}_{C6OL}$ = 4.1 kPa; N_2 balance].

at high conversions which enables the competing C=C bond migration route toward odd products (Scheme 1) and therefore explains the increasing Odd/Even ratio. The differences in the amount of odd and even C9–C24 products formed on the two samples results in a lower average molecular weight of the C9–C24 pool for sample 0.6CuMgAl (≈160–180 g/mol) than for 8.0CuMgAl (≈180–200 g/mol), Fig. 6 (open symbols).

To get more insight into the quality of the C9–C24 products obtained on both samples, the yield to oxygenates and hydrocarbons as well as the O/C atomic ratio were plotted in Fig. 7 as a function of conversion. The shape of the curves is consistent with oxygenates being primary products of the C6O pool conversion and hydrocarbons being formed consecutively from oxygenates, as postulated in Scheme 1. Thus, the hydrocarbon yield increased with X_{C6O} and represented about 20–40% of the C9–C24 pool at high conversions. Consequently, the O/C ratio decreased with conversion. The Cu loading affects not only the average molecular weight of the C9–C24 product pool but also the quality of the oxygenates; whereas C12 oxygenates were the main products on 0.6CuMgAl, heavier even and odd oxygenates formed on 8.0CuMgAl. Therefore, Fig. 7 shows that the O/C ratio decreased to a slightly lower value (0.04) on 0.6CuMgAl than on 8.0CuMgAl (0.06).

3.3. Mechanism and reaction pathways

In previous works we studied the coupling reactions of primary and secondary alcohols on Mg–Al mixed oxides with different Mg/Al ratios [14,41,53]. We showed that aldol condensation reactions require specific combinations of acid and base sites resulting from an adequate balance between Mg^{2+} and Al^{3+} cations. Thus, the active site is an acid-base pair ($M^{n+}-O^{2-}$, M = Lewis acid cation) in which oxygen presents moderate basic properties. Thus, a strong base such as MgO results, in general, less active than Mg-Al oxides with milder basic properties. On the other hand, an acidic oxide such as alumina is usually much more active than any Mg–Al oxide, but the selectivity to coupling products is negligible.

As we discussed above, an efficient catalyst for the upgrading of C6OL to liquid fuels must combine acid-base sites that promote aldol condensation steps and metallic sites that participate in hydro/dehydrogenation steps. A proper selection of these sites is necessary in order to avoid formation of unwanted products. For instance, both kinds of sites might promote the C—C bond cleavage reactions of C6OL and C6K, leading to light C3 compounds. Furthermore, acid-base properties must be balanced because weak acidity is needed for the dehydration of the aldol adducts but acid sites also promote the detrimental dehydration of C6OL to C6H.

Recently, using $ZCuM_I(M_{II})$ mixed oxide catalysts with ≈8 wt.% Cu and different acid-base properties we investigated the bifunctional nature of the catalytic process. These materials combine a metallic function supplied by Cu^0 atoms with acid-base properties provided by the metal cations M_I and M_{II} (M_I, M_{II}: Mg^{2+}, Al^{3+} or Ce^{4+}). The rate-limiting step (r.l.s.) operating on these solids was discussed by analyzing the turnover frequency (TOF) and site time yield to C9–C24 products per Cu^0 atom; we found that the r.l.s. changes depending on the oxide basicity [25].

Guisnet in a recent manuscript on the n-alkane hydroisomerization on bifunctional metal–acid zeolites, postulated the use of a plot of the TOF vs the site number ratio as a way to analyze how the balance between both sites affects the process rate-limiting step in different zeolites [54]. Following this approach, the site time yields to C9–C24 products (STY, s^{-1}) obtained with the ZCuMgAl catalysts were plotted in Fig. 8 as a function of the base/metal site ratio, n_b/n_{Cu^0} (closed squares). Since n_{Cu^0} could be measured only for ZCuMgAl catalysts with Z ⩾ 4.1 wt.% Cu, Table 1, the STY values were calculated for samples in that compositional region. The STY values of 9.8CuMg, 7.4CuCe, 6.4CuAl and 6.9CuMgCe oxides [25] were also plotted in Fig. 8 (open circles) showing that
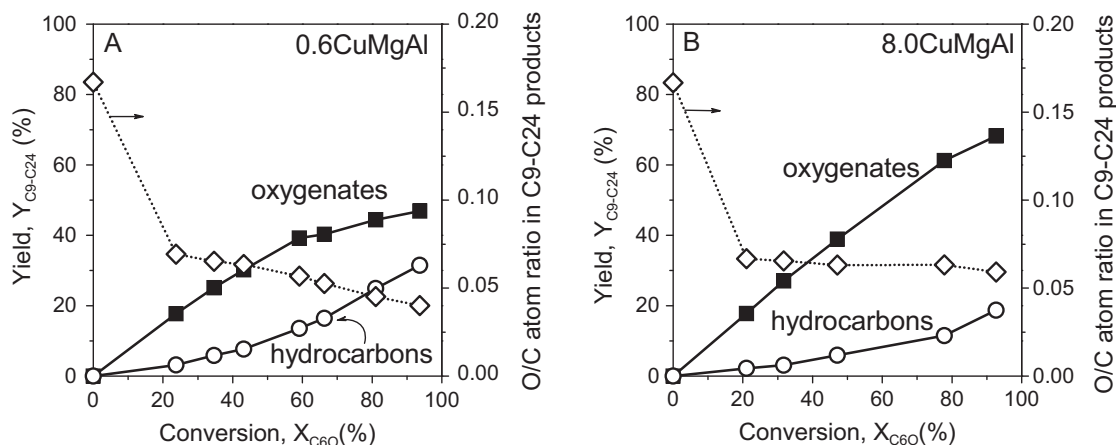
Fig. 7. Yield to oxygenates and hydrocarbons and O/C atom ratio in C9–C24 products as a function of conversion on (A) 0.6CuMgAl; (B) 8.0CuMgAl [T = 573 K, P = 101.3 kPa, $\bar{P}_{C6OL}$ = 4.1 kPa; N_2 balance].
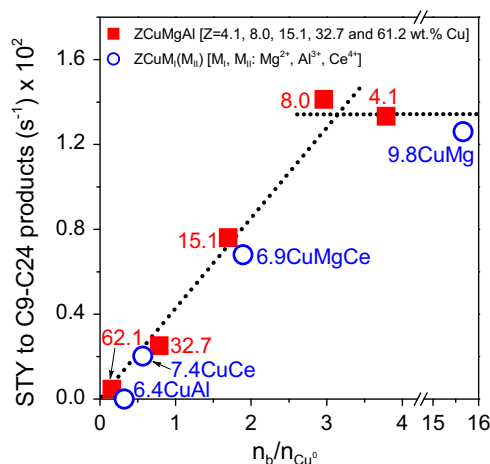
Fig. 8. Site time yield (STY) to C9–C24 products as a function of the base/metal site ratio (n_b/n_{Cu^0}) of ZCuMgAl and ZCuM$_I$(M$_{II}$) catalysts [T = 573 K, P = 101.3 kPa, $\bar{P}_{C6OL}$ = 4.1 kPa; N$_2$ balance].

regardless of the copper content or acid-base properties all the data points fell on the same curve.

The results of Fig. 8 show that the higher the copper content, the lower the specific yield to C9–C24 products. The shape of the STY vs n_b/n_{Cu^0} curve suggests that the r.l.s. changes as n_b/n_{Cu^0} becomes progressively larger. For catalysts with $n_b/n_{Cu^0} \leqslant 3$ the STY increased with increasing the proportion of base sites respect to the Cu^0 sites, indicating that on those solids a base-catalyzed reaction is rate limiting, i.e., the C—C bond forming step. The STY curve finally reached a constant value ($\approx$0.0135 s^{-1}) suggesting that catalysts with $n_b/n_{Cu^0} \approx$ 3–16 share the same rate-limiting step. Since the STY are calculated per surface Cu^0 sites, the similar STY values measured on catalysts with enhanced basic properties indicate that the process is limited by one of the Cu^0-promoted hydrogenation steps.

In summary, the synthesis of C9–C24 products on ZCuMgAl catalysts with $Z \geqslant 4.1$ wt.% Cu takes place through a bifunctional mechanism that involves both, acid-base pairs with basic properties and metal sites. However, the rate-limiting step depends on Z, i.e., on the relative abundance of surface Cu^0 species and M^{n+}–O^{2-} pairs. The experimental data provide evidence on the shift of the r.l.s. from a hydrogenation to an aldol condensation step as Z increases.

A question now arises concerning the mechanism of C9–C24 product formation that applies for catalysts with $Z < 4.1$ wt.% Cu. A closer inspection of Fig. 4C allows us to get insight into this issue. Formation of even carbon atom number oxygenates predominated on catalyst 0.3CuMgAl with C12O being the main product ($\approx$65% selectivity); but the selectivity gradually changed to odd products (C9O and C15O) as Z increased in that compositional zone. As can be seen in Scheme 1, after dehydrogenation of C6OL, formation of C12 oxygenates, especially C12UK^a, can occur without

participation of Cu^0 sites. Furthermore, the pathway toward odd products is promoted by M^{n+}–O^{2-} pairs and starts by C = C bond migration at the C12UK^a molecule. On the other hand, catalysts with $Z < 4.1$ wt.% Cu are hardly reducible under the reduction conditions used previous to the catalytic tests (573 K), as shown in Fig. 1, what suggests that the number of reduced copper species on the surface is probably scarce. In fact, TEM analysis (not shown) of samples 1.2CuMgAl and 1.8CuMgAl after reduction for 1 h in pure H$_2$ at 573 K showed the presence of small (3–4 nm) and scattered Cu^0 particles. However, observation of these particles is difficult because of the lack of enough image contrast. Thus, these samples probably contain a large number of partially reduced Cu^{n+} species that might behave as Lewis acid centers; Mg^{2+}, Al^{3+} and Cu^{n+} species would increasingly promote the C=C bond shift reaction toward odd products as Z increases in that compositional region.

We proved above that formation of C9–C24 products proceeds by a metal-base bifunctional mechanism on ZCuMgAl samples with high Cu loadings ($Z \geqslant 4.1$ wt.%). However, the characterization and catalytic results of the catalysts with $Z < 4.1$ wt.% Cu seem to suggest the existence of a conventional aldol condensation mechanism promoted by M^{n+}–O^{2-} pairs with moderate basic properties. In order to verify this, additional experiments were carried out in which selected ZCuMgAl catalysts with $Z < 4.1$ wt.% Cu were tested in the C6OL upgrading reaction but without a reduction pretreatment. Table 2 compares the results at 20% conversion for reduced and unreduced samples 0.3CuMgAl and 0.6CuMgAl. Results obtained with sample 0.3CuMgAl were almost independent of the existence or not of a reduction procedure, thereby reflecting the presence of a negligible amount of surface Cu^0 atoms after reduction at 573 K. Sample 0.6CuMgAl that contains a slightly higher Cu content, reduced to some extent at 573 K as indicated by the different C6OL/C6K and Odd/Even ratios measured for the reduced (0.06) and unreduced (0.37) sample experiments; this confirms that, in spite of a probably higher reducibility compared to sample 0.3CuMgAl, sample 0.6CuMgAl contains a higher number of not fully reduced Cu^{n+} species that enable the C=C bond migration pathway and therefore, odd compounds form with a higher selectivity. Similar effect occurs for the other samples with $Z < 4.1$ wt.%, as shown in Fig. 4C. Thus, on sample 0.3CuMgAl the synthesis of C9–C24 compounds seems to occur almost exclusively by base-catalyzed reaction steps such as dehydrogenation, aldol condensation and C=C bond migration. However, as Z increases in the $Z < 4.1$ wt.% Cu compositional zone, the ZCuMgAl samples reduce more easily and therefore, formation of C9–C24 compounds occurs through an increasing contribution of the bifunctional mechanism.

4. Conclusions

Cu–Mg–Al mixed oxides with a wide range of copper loadings (Z = 0.3–61.2 wt.% Cu) are active and selective for the upgrading of 2-hexanol toward liquid fuels, i.e., C9–C18+ compounds with

Table 2
Catalytic results for low Cu loading ZCuMgAl catalysts with different pretreatments.

Catalyst	Catalytic results							
	S_{C9-C24} (%) Reduction^a		S_{C6H} (%) Reduction^a		C6OL/C6K Reduction^a		Odd/Even C9–C24 Reduction^a	
	Yes	No	Yes	No	Yes	No	Yes	No
0.3CuMgAl	80	70	20	30	0.51	0.48	0.05	0.09
0.6CuMgAl	88	52	12	48	0.67	1.35	0.06	0.37

T = 573 K; $\bar{P}_{C6OL}$ = 4.1 kPa; N$_2$ balance; X_{C6O} = 20%.
^{a} T = 573 K; $\bar{P}_{H2}$ = 101.1 kPa.

low oxygen content. C9–C24 compounds are the main fraction with yields of up to 87%. This product pool is a hydrophobic mixture of compounds having one or none oxygen atom (ketones, alcohols and hydrocarbons), in which the O/C atom ratio is as low as 0.04.

Formation of C9–C24 compounds occurs through consecutive dehydrogenation, C—C bond formation, dehydration and hydrogenation steps. A bifunctional metal-base mechanism applies for high copper content Cu–Mg–Al mixed oxides in which nanosized Cu^0 particles promote dehydrogenation and hydrogenation steps and acid-base pairs with moderate basic properties catalyze the carbon chain lengthening reactions. Hydrogenation is rate-limiting on Cu–Mg–Al catalysts with enhanced basic properties (high base/metal site ratio). But as Z increases and consequently the base/metal site ratio decreases, the rate-limiting step shifts to the C—C bond formation reaction.

Products with odd carbon atom number are formed through a reaction pathway that starts by a C=C bond migration step promoted by acid-base sites such as the Mg(Al)–O pairs. Even carbon atom number products predominate on catalysts with a very low Cu content but the selectivity changes to odd products as the loading increases. This is attributed to the presence of partially reduced Cu^{n+} atoms that contribute as Lewis acid centers to the C=C bond shift. Low Cu loading Cu–Mg–Al mixed oxides are hardly reducible and therefore all the steps involved in the C9–C24 product formation are promoted mainly by acid-base sites.

Acknowledgements

Appendix A. Supplementary material

Supplementary data associated with this article can be found, in the online version, at http://dx.doi.org/10.1016/j.fuel.2016.02.084.

References

[1] Balakrishnan M, Sacia ER, Sreekumar S, Gunbas G, Gokhale AA, Scown CD, et al. Novel pathways for fuels and lubricants from biomass optimized using life-cycle greenhouse gas assessment. PNAS 2015;112(25):7645–9.

[2] Moomaw W, Burgherr P, Heath G, Lenzen M, Nyboer J, Verbruggen A. Annex II: Methodology. In: Edenhofer O, Pichs-Madruga R, Sokona Y, Seyboth K, Matschoss P, Kadner S, Zwickel T, Eickemeier P, Hansen G, Schlomer S, von Stechow C, editors. IPCC Special Report on Renewable Energy Sources and Climate Change Mitigation. Cambridge, United Kingdom and New York, USA: Cambridge University Press; 2011.

[3] Serrano-Ruiz JC, Dumesic JA. Catalytic routes for the conversion of biomass into liquid hydrocarbon transportation fuels. Energy Environ Sci 2011;4:83–99.

[4] Simonetti DA, Dumesic JA. Catalytic strategies for changing the energy content and achieving C–C coupling in biomass-derived oxygenated hydrocarbons. ChemSusChem 2008;1:725–33.

[5] Sacia ER, Deaner MH, Louie Y, Bell AT. Synthesis of biomass-derived methylcyclopentane as a gasoline additive via aldol condensation/hydrodeoxygenation of 2,5-hexanedione. Green Chem 2015;17:2393–7.

[6] Corma A, Iborra S, Velty A. Chemical routes for the transformation of biomass into chemicals. Chem Rev 2007;107:2411–502.

[7] Bond JQ, Alonso DM, Dumesic JA. Catalytic strategies for converting lignocellulosic carbohydrates to fuels and chemicals. In: Wyman CE, editor. Aqueous pretreatment of plant biomass for biological and chemical conversion to fuels and chemicals. UK: John Wiley & Sons, Ltd; 2013. p. 61–102.

[8] Milbrandt A, Kinchin C, McCormick R. The feasibility of producing and using biomass-based diesel and jet fuel in the United States. Technical Report NREL/TP-6A20-58015; 2013.

[9] Chheda JN, Dumesic JA. An overview of dehydration, aldol-condensation and hydrogenation processes for production of liquid alkanes from biomass-derived carbohydrates. Catal Today 2007;123:59–70.

[10] Kunkes EL, Simonetti DA, West RM, Serrano-Ruiz JC, Gärtner CA, Dumesic JA. Catalytic conversion of biomass to monofunctional hydrocarbons and targeted liquid-fuel classes. Science 2008;322:417–21.

[11] Sacia ER, Balakrishnan M, Deaner MH, Goulas KA, Toste FD, Bell AT. Highly selective condensation of biomass-derived methyl ketones as a source of aviation fuel. ChemSusChem 2015;8:1726–36.

[12] West RM, Kunkes EL, Simonetti DA, Dumesic JA. Catalytic conversion of biomass-derived carbohydrates to fuels and chemicals by formation and upgrading of mono-functional hydrocarbon intermediates. Catal Today 2009;147:115–25.

[13] Sankaranarayanapillai S, Sreekumar S, Gomes J, Grippo A, Arab GE, Head-Gordon M, et al. Catalytic upgrading of biomass-derived methyl ketones to liquid transportation fuel precursors by an organocatalytic approach. Angew Chem Int Ed 2015;54:4673–7.

[14] Di Cosimo JI, Torres G, Apesteguía CR. One-step MIBK synthesis: a new process from 2-propanol. J Catal 2002;208:114–23.

[15] Di Cosimo JI, Acosta A, Apesteguía CR. Gas-phase hydrogen transfer reduction of alfa, beta-unsaturated ketones on Mg-based catalysts. J Mol Catal A: Chem 2004;222:87–96.

[16] Torresi PA, Díez VK, Luggren PJ, Di Cosimo JI. Upgrading of diols by gas-phase dehydrogenation and dehydration reactions on bifunctional Cu-based oxides. Catal Sci Technol 2014;4:3203–13.

[17] Bravo-Suarez JJ, Subramaniam B, Chaudhari RV. Vapor-phase methanol and ethanol coupling reactions on CuMgAl mixed metal oxides. Appl Catal A: Gen 2013;455:234–46.

[18] Zhou M, Zeng Z, Zhu H, Xiao G, Xia R. Aqueous-phase catalytic hydrogenation of furfural to cyclopentanol over Cu–Mg–Al hydrotalcites derived catalysts: Model reaction for upgrading of bio-oil. J Energy Chem 2014;23:91–6.

[19] Jiang Z, Hao Z, Yu J, Hou H, Hu C, Su J. Catalytic combustion of methane on novel catalysts derived from Cu–Mg/Al-hydrotalcites. Catal Lett 2005;99:157–63.

[20] Tanasoi S, Tanchoux N, Urda A, Tichit D, Sandulescu I, Fajula F, et al. New Cu-based mixed oxides obtained from LDH precursors, catalysts for methane total oxidation. Appl Catal A: Gen 2009;363:135–42.

[21] Chmielarz L, Piwowarska Z, Rutkowska M, Wojciechowska M, Dudek B, Witkowski S, et al. Total oxidation of selected mono-carbon VOCs over hydrotalcite originated metal oxide catalysts. Catal Commun 2012;17:118–25.

[22] Xia S, Zheng L, Wang L, Chen P, Hou Z. Hydrogen-free synthesis of 1,2-propanediol from glycerol over Cu–Mg–Al catalysts. RSC Adv 2013;3:16569–76.

[23] Kannan S, Dubey A, Knozinger H. Synthesis and characterization of CuMgAl ternary hydrotalcites as catalysts for the hydroxylation of phenol. J Catal 2005;231:381–92.

[24] Barrault J, Derouault A, Courtois G, Maissant JM, Dupin JC, Guimon C, et al. On the catalytic properties of mixed oxides obtained from the Cu–Mg–Al LDH precursors in the process of hydrogenation of the cinnamaldehyde. Appl Catal A: Gen 2004;262:43–51.

[25] Luggren PJ, Apesteguía CR, Di Cosimo JI. Liquid transportation fuels from biomass-derived oxygenates: gas-phase 2-hexanol upgrading on Cu-based mixed oxides. Appl Catal A: Gen 2015;504:256–65.

[26] Luggren PJ, Apesteguía CR, Di Cosimo JI. Conversion of biomass-derived 2-hexanol to liquid transportation fuels: Study of the reaction mechanism on Cu–Mg–Al mixed oxides. Topics Catal 2015;59(2):196–206.

[27] Torresi PA, Díez VK, Luggren PJ, Di Cosimo JI. Conversion of diols by dehydrogenation and dehydration reactions on silica-supported copper catalysts. Appl Catal A: Gen 2013;458:119–29.

[28] Monti DA, Baiker A. Temperature-programmed reduction. Parametric sensitivity and estimation of kinetic parameters. J Catal 1983;83:323–35.

[29] Malet P, Caballero A. The selection of experimental conditions in temperature-programmed reduction experiments. J Chem Soc, Faraday Trans I 1988;84:2369–75.

[30] Sato S, Takahashi R, Sodesawa T, Yuma K, Obata Y. Distinction between surface and bulk oxidation of Cu through N_2O decomposition. J Catal 2000;196:195–9.

[31] Van Der Grift CJG, Wielers AFH, Joghi BPJ, Van Beijnum J, De Boer M, Versluijs-Helder M, et al. Effect of the reduction treatment on the structure and reactivity of silica-supported copper particles. J Catal 1991;131:178–89.

[32] Gervasini A, Bennici S. Dispersion and surface states of copper catalysts by temperature-programmed-reduction of oxidized surfaces (s-TPR). Appl Catal A: Gen 2005;281:199–205.

[33] Guerreiro ED, Gorriz OF, Rivarola JB, Arrúa LA. Characterization of Cu/SiO₂ catalysts prepared by ion-exchange for methanol dehydrogenation. Appl Catal A: Gen 1997;165:259–71.

[34] Bond GC, Namijo SN. An improved procedure for estimating the metal surface area of supported copper catalysts. J Catal 1989;118:507–10.

[35] Scanlon JT, Willis DE. Calculation of flame ionization detector relative response factors using the effective carbon number concept. J Chromatogr Sci 1985;23:333–9.

[36] Dietz WA. Response factors for gas chromatographic analyses. J Gas Chromatogr 1967;5:68–71.

[37] Kunkes EL, Gürbüz EI, Dumesic JA. Vapor-phase C–C coupling reactions of biomass-derived oxygenates over Pd/CeZrO_x catalysts. J Catal 2009;266:236–49.

[38] Díez VK, Torresi PA, Luggren PJ, Ferretti CA, Di Cosimo JI. Gas-phase conversion of 1,3-butanediol on single acid-base and Cu-promoted oxides. Catal Today 2013;213:18–24.

[39] Ferretti CA, Soldano A, Apesteguía CR, Di Cosimo JI. Monoglyceride synthesis by glycerolysis of methyl oleate on solid acid-base catalysts. Chem Eng J 2010;161:346–54.

[40] Díez VK, Apesteguía CR, Di Cosimo JI. Effect of the chemical composition on the catalytic performance. J Catal 2003;215:220–33.

[41] Di Cosimo JI, Díez VK, Xu M, Iglesia E, Apesteguía CR. Structure and surface and catalytic properties of Mg–Al basic oxides. J Catal 1998;78:499–510.

[42] Figueiredo RT, Martins Carvalho Andrade H, Fierro JLG. Low temperature water gas-shift catalysts. J Mole Catal A: Chem 2010;318:15–20.

[43] Gusi S, Trifiró F, Vaccari A. Kinetic study of the reduction of copper- zinc-aluminum mixed oxide catalysts. React Solids 1986;2:59–71.

[44] Database of Ionic Radii, <http://abulafia.mt.ic.ac.uk/shannon/>.

[45] Torres G, Apesteguía CR, Di Cosimo JI. One-step MIBK synthesis from 2-propanol: catalyst and reaction condition optimization. Appl Catal A: Gen 2007;317:161–70.

[46] Djinovic P, Levec J, Pintar A. Effect of structural and acidity/basicity changes of CuO–CeO$_2$ Catalysts on their activity for water–gas shift reaction. Catal Today 2008;138:222–7.

[47] Song F, Tan Y, Xie H, Zhang Q, Han Y. Direct synthesis of dimethyl ether from biomass-derived syngas over Cu–ZnO–Al$_2$O$_3$–ZrO$_2$(x)/γ-Al$_2$O$_3$ bifunctional catalysts: effect of Zr-loading. Fuel Process Technol 2014;126:88–94.

[48] Xu M, Gines MJL, Hilmen A, Stephens BL, Iglesia E. Isobutanol and methanol synthesis on copper catalysts supported on modified magnesium oxide. J Catal 1997;171:130–47.

[49] Di Cosimo I. Aldol reactions-Heterogeneous. In: Horváth IT, Iglesia E, Klein MT, Lercher JA, Russell AJ, Stiefel EI, editors. Encyclopedia of catalysis. USA: John Wiley and Sons; 2010.

[50] Olcay H, Subrahmanyam AV, Xing R, Lajoie J, Dumesic JA, Huber GW. Production of renewable petroleum refinery diesel and jet fuel feedstocks from hemicellulose sugar streams. Energy Environ Sci 2013;6:205–16.

[51] Díez VK, Apesteguía CR, Di Cosimo JI. Acid-base properties and active site requirements for elimination reactions on alkali-promoted MgO catalysts. Catal Today 2000;63:53–62.

[52] Choudhary TV, Phillips CB. Renewable fuels via catalytic hydrodeoxygenation. Appl Catal A: Gen 2011;397:1–12.

[53] Di Cosimo JI, Apesteguía CR, Ginés MJL, Iglesia E. Structural requirements and reaction pathways in condensation reactions of alcohols on Mg$_y$AlO$_x$ catalysts. J Catal 2000;190:261–75.

[54] Guisnet M. "Ideal" bifunctional catalysis over Pt-acid zeolites. Catal Today 2013;218–219:123–34.